

Low-Noise Cascaded Frequency Conversion of 637.2 nm Light to the Telecommunication C-Band in a Single-Waveguide Device

FABRICE VON CHAMIER,^{1,*} JOSCHA HANEL,¹ CHRIS MÜLLER,¹
WANRONG LI,¹ ROGER ALFREDO KÖGLER,¹ AND OLIVER BENSON¹

¹*Humboldt-Universität zu Berlin, Institut für Physik, Newtonstraße 15, 12489, Berlin, Germany*
**vonfabri@physik.hu-berlin.de*

Abstract: Interconnected quantum devices are the building blocks of quantum networks, where state transduction plays a central role. The frequency conversion of photons into the telecommunication C-band is decisive in taking advantage of current low-loss transmission lines. Here, we report the difference frequency conversion of 637.2 nm fluorescent light from a cluster of NV centers in diamond to tunable wavelengths between 1559.6 nm and 1565.2 nm. In order to avoid detrimental noise from spontaneous emissions, we use a two-step conversion device based on a single-pumped periodic poled lithium niobate waveguide. We observed a total external (internal) conversion efficiency of 3.0 ± 0.1 (20.5 ± 0.8) % with a noise rate of 2.4 ± 0.8 (16 ± 5) cps/GHz.

1. Introduction

Nitrogen-vacancy (NV) centers are suitable candidates for diverse quantum technology applications, ranging between single-photon emission [1], spin-photon entanglement [2] and quantum state storage [3]. The interconnection of such a platform to disparate sources or to different nodes of a quantum network [4–6] can take advantage of state transduction via quantum frequency conversion [7]. In this process, the quantum state of light is preserved, while its wavelength is shifted. Specifically, difference frequency generation (DFG) enables the compatibility of the zero-phonon emission line of NV centers at 637.2 nm with low-loss transmission networks and integrated technologies operating in the telecommunication bands [8, 9]. Combined with the incorporation of nanodiamonds in fibers [10], photonic crystals [11] and waveguides [12], low-noise frequency converters will play a fundamental role in the development of hybrid integrated photonic devices [13, 14].

Mediated by second-order nonlinearity ($\chi^{(2)}$), DFG is a three-wave mixing process that converts signal photons of frequency ω_s into a target frequency ω_t . Respecting energy conservation, the third frequency (pump) is fixed at $\omega_p = \omega_s - \omega_t$. Additionally, the phase-matching condition $\vec{k}_p = \vec{k}_s - \vec{k}_t$ must be satisfied, where \vec{k}_i , $i = \{s, t, p\}$ is the wave vector. Such a condition is not trivially reached, but quasi-phase matching can be guaranteed for high efficiency conversion by periodic poling techniques [15, 16].

Periodic poled lithium niobate (PPLN) crystals and waveguides are widely used in $\chi^{(2)}$ nonlinear optics applications, including photon sources [17, 18], generation of squeezed light [19, 20] and quantum frequency converters [8, 9, 21–33]. This photonic platform is particularly promising due to its strong nonlinear coefficient, wide optical transparency window, large refractive index, and high electro-optical effect [34]. Waveguide structures have the additional advantage of being compatible with integrated devices [13, 14]. The preservation of non-classical states after DFG conversion in PPLN waveguides was demonstrated for photons generated on different platforms, such as ion traps [22–24], quantum dots [25–29], devices based on spontaneous parametric down-conversion (SPDC) [30, 31] and defect centers in diamonds [9, 32, 33]. These results compile successful conversion to target frequencies in the telecommunication O-, C-, and L-bands.

In general, intense pump fields are necessary to efficiently convert photons. In this strong pump regime, excessive background noise due to spontaneous effects, mainly SPDC [35, 36] and Raman scattering [37–41], increases the noise spectral density at target frequencies. A possible strategy to overcome this issue relies on cascaded conversion. By introducing intermediate converted colors, the pump can be highly separated from the target wavelength. This is a viable approach for bypassing the detrimental effects of background noise photons [42]. Two-step DFG was successfully employed for the low-noise conversion of 650 nm photons to 1588 nm, within the telecom L-band, in a dual-pumped integrated device [42]. Furthermore, photons from trapped ions [27, 28] and silicon vacancy centers [32] were converted to telecom bands using two separated waveguide systems for two-step conversion.

Here, we demonstrate the conversion of 637.2 nm signals into the telecommunication C-band using a two-stage DFG process in a highly integrated device, i.e., a single-pumped two-section PPLN waveguide. We successfully convert fluorescence photons from NV centers in diamond to the telecommunication C-band with an external (internal) conversion efficiency of 3.0 ± 0.1 (20.5 ± 0.8) % and a background noise rate of 2.4 ± 0.8 (16 ± 5) cps/GHz. The overall losses in our system precluded the operation of the device at single-photon levels. We note that a similar system was recently reported for the conversion of 637 nm light to the L-band with equivalent noise levels [43].

2. Experimental Methods

Our frequency conversion device consists of an NTT Electronics PPLN on lithium tantalate ridge waveguide with two different periodic poling sections. Each domain of the 40 mm long waveguide is equally divided in 20 mm segments and both facets are anti-reflective coated in an effort to minimize coupling losses. In order to avoid photorefractive damage at room temperature, the lithium niobate is doped with 5 mol% ZnO [44]. The device is glued on a copper tellurium base and mounted in 2 copper casings, where the temperature of each section is actively stabilized with Peltier elements localized underneath them.

The experimental setup is summarized in figure 1. The pump field is generated by a $\text{Cr}^{2+}:\text{ZnS}$ laser, tunable between 1980 nm and 2528 nm. Signal and pump are combined with the dichroic mirror (DM1) and coupled to the two-step conversion PPLN waveguide with the aid of an uncoated aspheric lens. The signal fiber output provides light emitted either from a reference laser or from a cluster of NV centers in diamond. The movable mirror M1 allows the coupling of an auxiliary signal at 905.1 nm used to evaluate the second-step conversion internal efficiency. Pump, signal and auxiliary signal are coupled to the waveguide with respective efficiencies of 74.5 %, 88.2 % and 81.8 %.

A second uncoated aspheric lens collimates the out-coupled light into free space, where the four fields involved in the two-step DFG are separated with a combination of dichroic mirrors (DMs). Photodiodes (PDs) are used to monitor the pump, signal and intermediary conversion step fields. The target wavelength is sent to a superconductive nanowire single photon detector (SNSPD), allowing the detection of low-intensity conversion. Stacked free-space bandpass filters (BPFs) reduce the contribution of pump photons to the detection background noise. The tunable bandpass filter has an adjustable bandwidth as narrow as 32 pm and ranges from 1480 nm to 1620 nm, enabling the spectral characterization of the converted light through almost the entire telecommunication band. The movable mirror M2 is used for coupling the waveguide output into an optical spectrum analyzer (OSA) (Yokogawa AQ6370D).

Optimal phase-matching conditions in the frequency converter can be achieved by tuning the temperatures of the Peltier elements on each section of the waveguide. Figure 2 shows the calculated phase-matching condition for both steps at different temperatures. The reference values for the theoretical plot followed the Sellmeier coefficients for lithium niobate and lithium tantalate, as provided in [45] and [46], respectively. Dispersion effects were considered, where

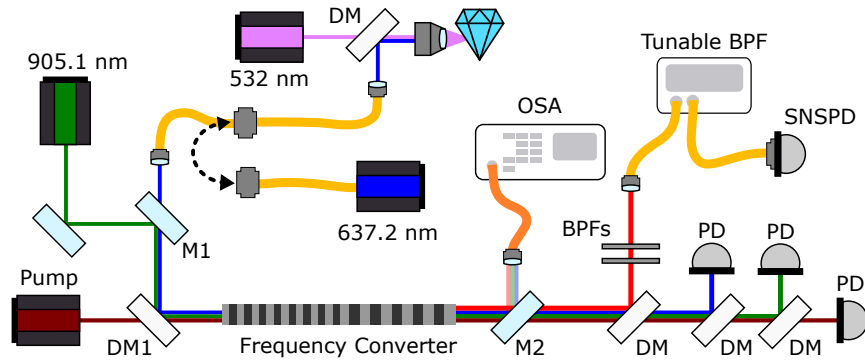


Fig. 1. Simplified optical setup. The signal can be taken as either a tunable laser centered at 637.2 nm or the fluorescence of a cluster of NV centers in diamond. 637.2 nm or 905.1 nm are independently combined with the pump laser and send to the conversion system. After the frequency converter, the output fields are either sent to an optical spectrum analyzer (OSA) or are separated for individual detection. M: movable mirror, DM: dichroic mirror, BPF: bandpass filter, PD: photodiode, SNSPD: superconducting nanowire single photon detector.

finite-difference time-domain simulations were used to determine the effective refractive index of the propagating fields.

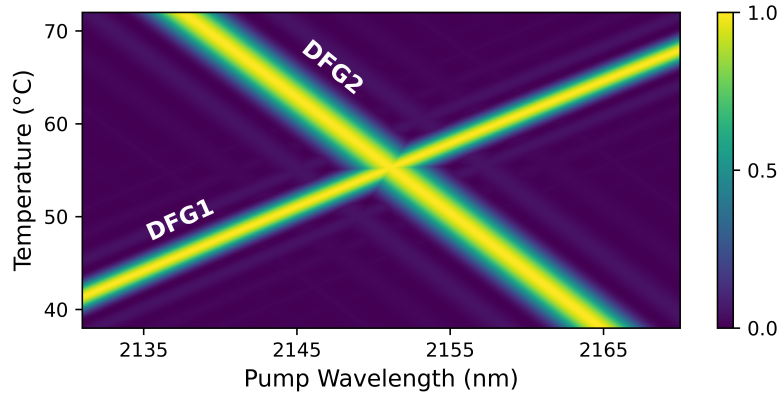


Fig. 2. Phase-matching tuning of the two-step conversion. The conversion efficiency heatmaps of the first- (DFG1) and second-step (DFG2) conversion are shown as a function of each step temperature and the pump wavelength.

3. Results and Discussion

In order to avoid detrimental effects on the conversion efficiency due to temperature gradients, we tuned our experiment to a configuration where the first- and second-step conversions are phase-matched to the same temperature. After fine-tuning the pump wavelength to 2152.9 nm and the crystal temperature to 59.26 °C, we successfully converted 637.2 nm photons to 905.1 nm followed by a conversion to 1561.6 nm. This condition slightly differs from the expected degenerate temperature phase-matching conditions of figure 2 due to experimental variations, such as temperature gradients between the waveguide and the temperature sensors, deviations

from the calculated refractive indexes, surface roughness and nonparallel walls in our waveguide system.

Optimal mode matching was ensured by measuring the transverse profile of the coupled beams after free space out-coupling and by evaluating the first-step conversion of a strong signal field with the aid of a photodetector. Figure 3 shows the expected conversion proportional to $\text{sinc}^2(\Delta k L/2)$, where the phase mismatch (Δk) was tuned with the pump wavelength and L is the length of the phase-matched section of the waveguide respective to the first DFG. A remaining conversion of higher order mode is still visible and the profiles of the modes are depicted in figure 3 inset.

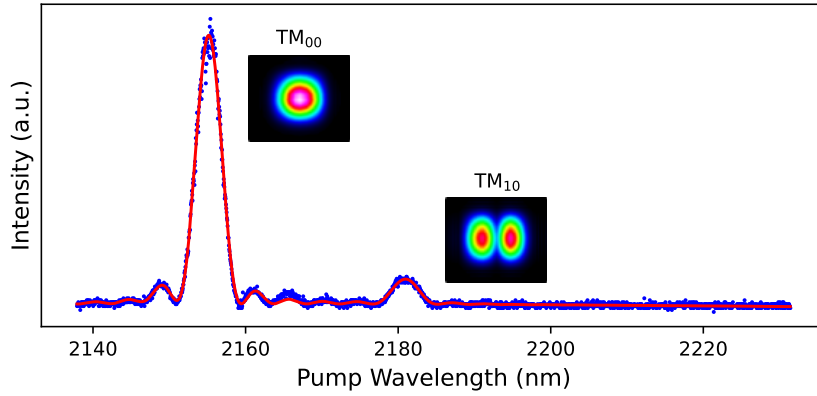


Fig. 3. Intensity of the generated light in the first-step conversion to 905.1 nm as a function of the pump wavelength. The indicated modes were verified with a beam profiler and are shown in the graphic inset.

The first-step internal conversion efficiency was determined by monitoring the depletion of the 637.2 nm signal after the waveguide out-coupling. For the investigation of the second-step, we used the auxiliary laser tuned to 905.1 nm, which corresponds to the wavelength of the conversion of 637.2 nm light after the first-step conversion. As the auxiliary frequency is also phase-matched to the first-step conversion, sum frequency generation (SFG) is expected, which jeopardizes a depletion measurement. However, because SFG has a narrower phase-matching region than DFG, we were able to suppress it with a small shift on the pump wavelength at the cost of underestimating the second-step conversion efficiency. Figure 4 (a) shows the internal conversion efficiencies as a function of the power of the out-coupled pump. The data is fitted to the equation $\eta_{int} \propto \sin^2(\sqrt{\eta_{nor} P_p L})$ [39], where η_{nor} is the normalized efficiency (in unit per Watt per millimeter squared). The curves indicate our limitation in the coupled pump power, which hinders higher conversion efficiencies. As maximum conversion cannot be achieved in either of the conversion processes, these values cannot be precisely determined.

The total efficiency fitted to the product of the conversion functions is shown in figure 4 (b), reaching an external conversion efficiency limited to 3.0 ± 0.1 % corresponding to an out-coupled pump power of 225 mW. This value was reached by comparing the total photon number of a strong signal coupled into the waveguide with the number of converted photons after our filtering system. The power measurements were performed with the aid of a power meter. In order to isolate the converted photons from remaining pump photons and any detrimental background noise, we used stacked BPFs centered at 1550 nm with 40 nm FWHM followed by a 32 pm tunable filter centered at the target wavelength of 1561.6 nm. The total losses at this wavelength sum up to 85.4 ± 0.1 % and have contributions of the out-coupling efficiency (92.2 ± 0.2 %),

free-space filters and optical elements transmission ($94.7 \pm 0.2 \%$), SMF coupling efficiency ($82.6 \pm 0.1 \%$) and tunable BPF transmission ($20.2 \pm 0.1 \%$). Accounting for the losses, we obtain a maximum internal conversion of $20.5 \pm 0.8 \%$, limited by the accessible pump power.

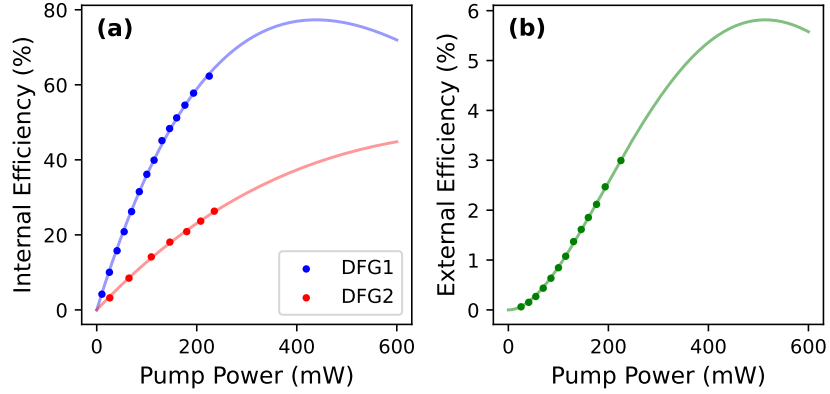


Fig. 4. Conversion efficiencies of the two-step converter. DFG1 is the conversion from 637.2 nm to 905.1 nm and DFG2 is the conversion from 905.1 nm to 1561.6 nm. (a) Internal conversion efficiencies of the individual steps measured after the waveguide out-coupling. (b) External conversion efficiency of the cascaded process.

As a next step we investigated the tuning capability of our device. Following the phase-matching conditions of figure 2 we were able to tune the target wavelength by shifting the temperature of the second poling section of the converter away from the temperature degeneracy point. With a gradient of $\Delta T = 4.6 \text{ }^\circ\text{C}$ we reached a target wavelength of 1559.0 nm with an external conversion efficiency of $2.8 \pm 0.3 \%$. Furthermore, by setting $\Delta T = -6.1 \text{ }^\circ\text{C}$, the reached configuration was 1564.9 nm with $2.9 \pm 0.2 \%$ of efficiency. Despite the temperature gradients induced between the poled sections the conversion efficiency remained within the error margins in this tuning range. The tunability limits were not explored in order to avoid damages to the chip due to physical stress.

The overall spectrum of the device output shown in figure 5 was measured with an OSA, where we verified all the involved fields in our conversion process within the equipment range. The peak at 1076.5 nm is due to second harmonic generation of the pump in the waveguide, where its expected quadratic response with the pump power [47] was experimentally verified.

We thoroughly investigated the target spectrum around the wavelength of 1561.6 nm (inset in figure 5) using the combination of the tunable BPF and an SNSPD. Noise near the target wavelength is a critical limitation of frequency converters. Therefore, we characterized the noise spectral density of our system by setting the tunable BPF to the target wavelength with minimum bandwidth (4 GHz). Taking an integration time of 20 minutes, we reached a total count rate of 142 ± 1 cps, of which 135 ± 2 cps are attributed to dark counts. Accounting for the SNSPD detection efficiency of $72 \pm 3 \%$, we reach a pump induced noise count rate of 10 ± 3 cps, corresponding to an external noise spectral density of 2.4 ± 0.8 cps/GHz. Correcting for the system external losses, we obtain an internal noise spectral density of 16 ± 5 cps/GHz. The background noise is comparable to that of other reported two-step conversion schemes [28, 32, 42, 43], while the device itself is more compactly designed.

A prominent feature near the target wavelength is a broad peak centered at 1532.8 nm. Further investigations into the source of this contribution to noise led to a process occurring in the waveguide independently from the signal field. This is a phase-matched conversion related to the second-step periodic poling, where its central wavelength shifted linearly by $-0.045 \text{ nm}/^\circ\text{C}$ within

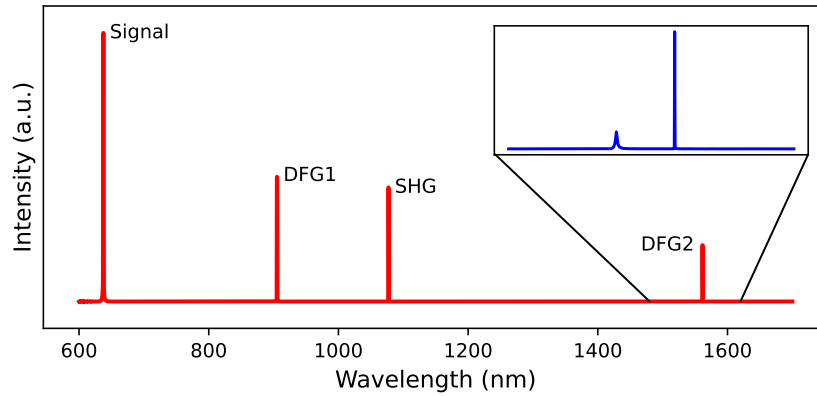


Fig. 5. Optical spectrum of the converter output. First (DFG1) and second (DFG2) frequency difference generation steps are indicated in the figure, as well as the second harmonic generation (SHG) of the pump field. The inset shows the spectral region from 1480 nm to 1620 nm, measured with the combination of the tunable BPF with the SNSPD, unraveling an extra peak near DFG2.

a 10 °C temperature detuning range. Its frequency also scales linearly with the pump wavelength, remaining at a constant separation of 56.34 ± 0.01 THz. The efficiency of the generated peak is highly dependent on the polarization of the pump, further indicating its relation to the periodic poling structure. Such temperature and strong polarization dependence discards the possibility of a pure Raman scattering origin. Finally, the process showed a linear dependence with the pump intensity, eliminating any wave mixing processes between different pump harmonics. The origin of this peak is then attributed to SFG of the pump combined with thermal photons in the range of $5.3 \mu\text{m}$.

We were able to confirm this speculation by a theoretical model. The detailed line shape of the converted thermal photons is shown in figure 6. Note that we displaced its center wavelength from 1532.8 nm to the center of the free-space BPFs at 1550 nm in order to avoid any distortions caused by the filter cutoff. Assuming that the thermal emission can be described by black body

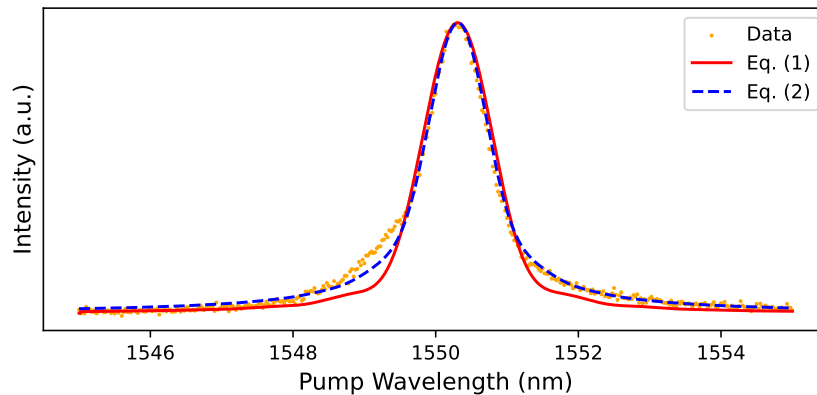


Fig. 6. Noise peak caused by thermal photons converted by SFG. The different fittings are given by the analytical model of Eq. (1) and the numerical modification of Eq. (2).

radiation, the mid-infrared spectrum remains flat. Hence, an underlying phase-matching curve of the form $\text{sinc}^2(\Delta kL/2)$ is expected. Considering, however, that the thermal photons are generated at different positions along the waveguide, the total output intensity will be given by [48]

$$I \propto \int_0^L \frac{(L-z)^2}{L} \text{sinc}^2\left(\frac{\Delta k(L-z)}{2}\right) dz$$

$$= \frac{2}{\Delta k^2} [1 - \text{sinc}(\Delta kL)].$$
(1)

Note that we did not consider any contribution from the first half of the waveguide to the thermal photons, as lithium niobate is highly absorptive for this frequency range [49]. The fitting of the analytical model is shown in figure 6, which is in good agreement with the data. The deviation in the tails of the function is due to the assumption of a uniform distribution of thermal photons along the waveguide. A better description of the noise peak is numerically obtained by including weighting parameters along the waveguide length according to

$$I \propto \sum_z \sum_{i=0}^n a_i z^i \text{sinc}^2\left(\frac{\Delta kz}{2}\right),$$
(2)

where $z \in [0, L]$, a_i is the free parameter and we chose $n = 2$ to avoid over fitting. The asymmetry of the peak is likely due to non-uniformities in the waveguide.

A targeted task of our converter is to convert photons from NV centers to the telecom C-band. Therefore, as a final demonstration, we converted fluorescence photons collected from a cluster of NV centers in diamond with a confocal microscope configuration [50], as represented in figure 1. We off-resonantly excite the defect centers with a 532 nm pump and connect the collected photons to the converter with a SMF. The spectrum of the color centers emission is shown in figure 7 (a), where the zero-phonon line is indicated at 637.2 nm. The resulting spectrum after the cascaded conversion process is shown in figure 7 (b). The characteristic sinc^2 function can be faintly seen after conversion, as the fluorescence spectrum of the bulk diamond is much broader than the conversion bandwidth.

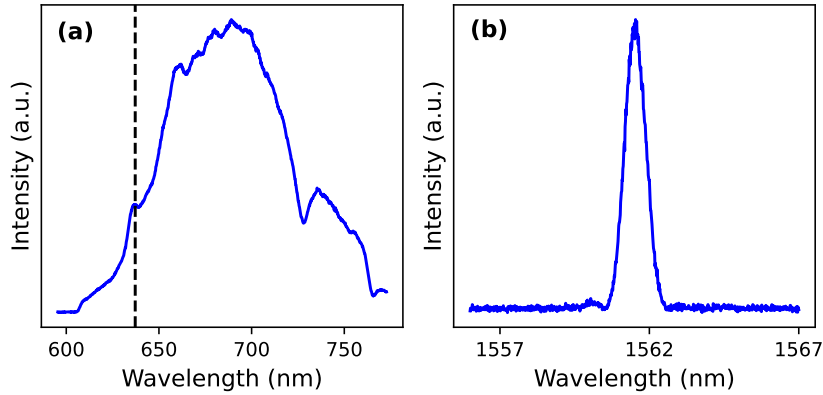


Fig. 7. Cascaded conversion of fluorescence light from NV centers in diamond. (a) Fluorescence spectrum of the optical source. The vertical line indicates the zero-phonon line. (b) Converted spectrum from the surroundings of the zero-phonon line to telecommunication C-band frequencies.

Given the efficiency of our two-step conversion and the overall loss budget from the confocal microscope to the frequency converter device, a significant number of NV centers contributed

to the fluorescence signal, resulting in approximately $10 \mu\text{W}$ of optical power. Nonetheless, the frequency conversion of non-classical states in similar compact devices would benefit from the achieved low-noise performance. Further improvements in conversion efficiency, attainable through asymmetric poling lengths, would enable the conversion of signals in the single-photon regime. Additionally, the conversion of thermal photons can be suppressed by redesigning the poling periods. An elaborated discussion on the limits of single-photon frequency conversion can be found in reference [8].

4. Conclusion

We experimentally demonstrated the two-step conversion of light emitted by NV centers in diamond to the telecommunication C-band, where we used a single-pumped waveguide device. The tunability of the system was demonstrated by changing the phase-matching conditions with temperature control of the individual DFG steps. This feature can be further optimized with thermally isolated poled sections and can be precisely controlled with the aid of localized microheaters [51]. We observed a total external (internal) conversion efficiency of 3.0 ± 0.1 (20.5 ± 0.8)%. Higher efficiencies can be reached with asymmetric poling lengths, individually optimized to each conversion step. Our cascaded two-step conversion in a single waveguide not only provides a highly integrated approach, but at the same time it reduces the background noise from Raman scattering and SPDC. We observed an external (internal) noise spectral density of 2.4 ± 0.8 (16 ± 5) cps/GHz, which is on par with other reported quantum converters. The low background noise can be attributed to remaining anti-Stokes Raman scattering of the pump [41]. Surprisingly, phase-matched SFG of thermal photons provided a significant contribution to the noise as we investigated in detail experimentally and theoretically. This can be bypassed by choosing different poling periods, however it is important to take this extra noise source into account when designing future integrated conversion devices.

Funding. This project was funded by BMBF, QR.X project 16KISQ003. R.A.K. acknowledges funding by the Senat Berlin.

Acknowledgment. We thank Tim Kroh for his contributions to early implementations of the project and Sven Ramelow and Felix Mann for valuable discussions and insights on the converted spectrum.

Disclosures. The authors declare no conflicts of interest.

Data Availability Statement. Data underlying the results presented in this paper are not publicly available at this time but may be obtained from the authors upon reasonable request.

References

1. C. Kurtsiefer, S. Mayer, P. Zarda, and H. Weinfurter, "Stable solid-state source of single photons," *Phys. review letters* **85**, 290 (2000).
2. E. Togan, Y. Chu, A. S. Trifonov, *et al.*, "Quantum entanglement between an optical photon and a solid-state spin qubit," *Nature* **466**, 730–734 (2010).
3. G. Fuchs, G. Burkard, P. Klimov, and D. Awschalom, "A quantum memory intrinsic to single nitrogen–vacancy centres in diamond," *Nat. Phys.* **7**, 789–793 (2011).
4. H. J. Kimble, "The quantum internet," *Nature* **453**, 1023–1030 (2008).
5. S. Wehner, D. Elkouss, and R. Hanson, "Quantum internet: A vision for the road ahead," *Science* **362**, eaam9288 (2018).
6. A. J. Stolk, K. L. van der Enden, M.-C. Slater, *et al.*, "Metropolitan-scale heralded entanglement of solid-state qubits," *Sci. advances* **10**, eadp6442 (2024).
7. P. Kumar, "Quantum frequency conversion," *Opt. letters* **15**, 1476–1478 (1990).
8. R. Ikuta, T. Kobayashi, S. Yasui, *et al.*, "Frequency down-conversion of 637 nm light to the telecommunication band for non-classical light emitted from nv centers in diamond," *Opt. express* **22**, 11205–11214 (2014).
9. A. Dréau, A. Tchegbotareva, A. E. Mahdaoui, *et al.*, "Quantum frequency conversion of single photons from a nitrogen-vacancy center in diamond to telecommunication wavelengths," *Phys. review applied* **9**, 064031 (2018).
10. T. Schroder, A. W. Schell, G. Kewes, *et al.*, "Fiber-integrated diamond-based single photon source," *Nano letters* **11**, 198–202 (2011).

11. A. Faraon, C. Santori, Z. Huang, *et al.*, “Coupling of nitrogen-vacancy centers to photonic crystal cavities in monocrystalline diamond,” *Phys. review letters* **109**, 033604 (2012).
12. A. Faraon, C. Santori, Z. Huang, *et al.*, “Quantum photonic devices in single-crystal diamond,” *New J. Phys.* **15**, 025010 (2013).
13. A. W. Elshaari, W. Pernice, K. Srinivasan, *et al.*, “Hybrid integrated quantum photonic circuits,” *Nat. photonics* **14**, 285–298 (2020).
14. J.-H. Kim, S. Aghaieibodi, J. Carolan, *et al.*, “Hybrid integration methods for on-chip quantum photonics,” *Optica* **7**, 291–308 (2020).
15. J. Armstrong, N. Bloembergen, J. Ducuing, and P. S. Pershan, “Interactions between light waves in a nonlinear dielectric,” *Phys. review* **127**, 1918 (1962).
16. P. Franken and J. F. Ward, “Optical harmonics and nonlinear phenomena,” *Rev. Mod. Phys.* **35**, 23 (1963).
17. F. König, E. J. Mason, F. N. Wong, and M. A. Albota, “Efficient and spectrally bright source of polarization-entangled photons,” *Phys. Rev. A — At. Mol. Opt. Phys.* **71**, 033805 (2005).
18. M. Bock, A. Lenhard, C. Chunnillall, and C. Becher, “Highly efficient heralded single-photon source for telecom wavelengths based on a ppln waveguide,” *Opt. express* **24**, 23992–24001 (2016).
19. J. Feng, X. Tian, Y. Li, and K. Zhang, “Generation of a squeezing vacuum at a telecommunication wavelength with periodically poled linbo₃,” *Appl. Phys. Lett.* **92** (2008).
20. T. Kashiwazaki, N. Takanashi, T. Yamashima, *et al.*, “Continuous-wave 6-db-squeezed light with 2.5-thz-bandwidth from single-mode ppln waveguide,” *APL Photonics* **5** (2020).
21. F. Mann, H. M. Chrzanowski, F. Gewers, *et al.*, “Low-noise quantum frequency conversion in a monolithic cavity with bulk periodically poled potassium titanyl phosphate,” *Phys. Rev. Appl.* **20**, 054010 (2023).
22. T. Walker, K. Miyanishi, R. Ikuta, *et al.*, “Long-distance single photon transmission from a trapped ion via quantum frequency conversion,” *Phys. review letters* **120**, 203601 (2018).
23. V. Krutyanskiy, M. Meraner, J. Schupp, *et al.*, “Light-matter entanglement over 50 km of optical fibre,” *npj Quantum Inf.* **5**, 72 (2019).
24. M. Meraner, A. Mazloom, V. Krutyanskiy, *et al.*, “Indistinguishable photons from a trapped-ion quantum network node,” *Phys. Rev. A* **102**, 052614 (2020).
25. K. De Greve, L. Yu, P. L. McMahon, *et al.*, “Quantum-dot spin–photon entanglement via frequency downconversion to telecom wavelength,” *Nature* **491**, 421–425 (2012).
26. B. Kambs, J. Kettler, M. Bock, *et al.*, “Low-noise quantum frequency down-conversion of indistinguishable photons,” *Opt. express* **24**, 22250–22260 (2016).
27. J. Hannegan, U. Saha, J. D. Siverns, *et al.*, “C-band single photons from a trapped ion via two-stage frequency conversion,” *Appl. Phys. Lett.* **119** (2021).
28. U. Saha, J. D. Siverns, J. Hannegan, *et al.*, “Low-noise quantum frequency conversion of photons from a trapped barium ion to the telecom o-band,” *ACS Photonics* **10**, 2861–2865 (2023).
29. J. H. Weber, B. Kambs, J. Kettler, *et al.*, “Two-photon interference in the telecom c-band after frequency conversion of photons from remote quantum emitters,” *Nat. nanotechnology* **14**, 23–26 (2019).
30. T. Kroh, A. Ahlrichs, B. Sprenger, and O. Benson, “Heralded wave packet manipulation and storage of a frequency-converted pair photon at telecom wavelength,” *Quantum Sci. Technol.* **2**, 034007 (2017).
31. A. Lenhard, J. Brito, M. Bock, *et al.*, “Coherence and entanglement preservation of frequency-converted heralded single photons,” *Opt. express* **25**, 11187–11199 (2017).
32. M. Schäfer, B. Kambs, D. Herrmann, *et al.*, “Two-stage, low noise quantum frequency conversion of single photons from silicon-vacancy centers in diamond to the telecom c-band,” *Adv. Quantum Technol.* p. 2300228 (2023).
33. E. Bersin, M. Sutula, Y. Q. Huan, *et al.*, “Telecom networking with a diamond quantum memory,” *PRX Quantum* **5**, 010303 (2024).
34. Y. Qi and Y. Li, “Integrated lithium niobate photonics,” *Nanophotonics* **9**, 1287–1320 (2020).
35. J. S. Pelc, C. Langrock, Q. Zhang, and M. M. Fejer, “Influence of domain disorder on parametric noise in quasi-phase-matched quantum frequency converters,” *Opt. letters* **35**, 2804–2806 (2010).
36. H. Takesue, “Single-photon frequency down-conversion experiment,” *Phys. Rev. A — At. Mol. Opt. Phys.* **82**, 013833 (2010).
37. C. Langrock, E. Diamanti, R. V. Roussev, *et al.*, “Highly efficient single-photon detection at communication wavelengths by use of upconversion in reverse-proton-exchanged periodically poled linbo 3 waveguides,” *Opt. letters* **30**, 1725–1727 (2005).
38. P. S. Kuo, J. S. Pelc, O. Slattery, *et al.*, “Reducing noise in single-photon-level frequency conversion,” *Opt. letters* **38**, 1310–1312 (2013).
39. S. Zaske, A. Lenhard, and C. Becher, “Efficient frequency downconversion at the single photon level from the red spectral range to the telecommunications c-band,” *Opt. express* **19**, 12825–12836 (2011).
40. S. Zaske, A. Lenhard, C. A. Keßler, *et al.*, “Visible-to-telecom quantum frequency conversion of light from a single quantum emitter,” *Phys. review letters* **109**, 147404 (2012).
41. J. S. Pelc, L. Ma, C. Phillips, *et al.*, “Long-wavelength-pumped upconversion single-photon detector at 1550 nm: performance and noise analysis,” *Opt. express* **19**, 21445–21456 (2011).
42. V. Esfandyarpour, C. Langrock, and M. Fejer, “Cascaded downconversion interface to convert single-photon-level signals at 650 nm to the telecom band,” *Opt. Lett.* **43**, 5655–5658 (2018).

43. F. Elsen, B. Jungbluth, J. F. Geus, *et al.*, “Dual approaches for the development of robust, scalable, ultra-low-noise quantum frequency converters for nv center qubits,” in *Quantum 2.0*, (Optica Publishing Group, 2024), pp. QTu4A–5.
44. D. Bryan, R. Gerson, and H. Tomaschke, “Increased optical damage resistance in lithium niobate,” *Appl. Phys. Lett.* **44**, 847–849 (1984).
45. D. H. Jundt, “Temperature-dependent sellmeier equation for the index of refraction, n_e , in congruent lithium niobate,” *Opt. letters* **22**, 1553–1555 (1997).
46. N. Barboza and R. Cudney, “Improved sellmeier equation for congruently grown lithium tantalate,” *Appl. Phys. B* **95**, 453–458 (2009).
47. M. M. Fejer, G. Magel, D. H. Jundt, and R. L. Byer, “Quasi-phase-matched second harmonic generation: tuning and tolerances,” *IEEE J. quantum electronics* **28**, 2631–2654 (1992).
48. C. Pedersen, Q. Hu, L. Høgstedt, *et al.*, “Non-collinear upconversion of infrared light,” *Opt. Express* **22**, 28027–28036 (2014).
49. M. Leidinger, S. Fieberg, N. Waasem, *et al.*, “Comparative study on three highly sensitive absorption measurement techniques characterizing lithium niobate over its entire transparent spectral range,” *Opt. express* **23**, 21690–21705 (2015).
50. T. Schröder, F. Gädeke, M. J. Banholzer, and O. Benson, “Ultrabright and efficient single-photon generation based on nitrogen-vacancy centres in nanodiamonds on a solid immersion lens,” *New J. Phys.* **13**, 055017 (2011).
51. B. S. Lee, M. Zhang, F. A. Barbosa, *et al.*, “On-chip thermo-optic tuning of suspended microresonators,” *Opt. Express* **25**, 12109–12120 (2017).